Research Article

Ya-Nan Sun, Shen-Jiang Wu*, Guo-Sheng Qin, Ke-Xuan Wang, Jia Wang, Dang-Juan Li, and Yu-Qi Du

Weak beat frequency extraction method for photon Doppler signal with low signal-to-noise ratio

https://doi.org/10.1515/phys-2023-0172
received October 11, 2023; accepted December 21, 2023

Abstract: In the window function spectrum of the low signal-to-noise ratio photon Doppler signal after the short-time Fourier transform, the weak beat frequency cannot be obtained by extracting the maximum amplitude spectrum frequency of each window because the amplitude of the noise spectrum exceeds the weak beat frequency. In this article, the value of the beat frequency is first estimated by the Kalman filter. Then, a multiple analytical bandpass filter is constructed to refine the spectrum of the high noise signal with the value of the beat frequency estimate as the spectrum band center. This technique extracts only the beat frequencies from the narrowband refinement spectrum by removing the interference spectrum band range. We use this technique to process the photon Doppler signals from the tiny high-speed flying fragments explosion experiment. After data processing, the beat frequency value heavily affected by high-frequency noise can reduce the error by up to 64.9%. The beat frequency value of the low noise signal can be accurate to 10^6 Hz, equivalent to 0.775 m/s after velocity demodulation. This method fully considers the positioning and protection of the beat frequency characteristics. It makes weak beat frequencies more obvious in the refined narrowband spectrum without changing the signal amplitude. This article describes a method for extracting the weak beat frequency of the photon Doppler signal or a signal optimization algorithm for needing high-precision beat frequencies in a test environment.

*** Corresponding author: Shen-Jiang Wu**, School of Optoelectronic Engineering, Xi'an Technological University, Xi'an, 710021, China, e-mail: bxait@xatu.edu.cn
Ya-Nan Sun, **Jia Wang**, **Dang-Juan Li**, **Yu-Qi Du:** School of Optoelectronic Engineering, Xi'an Technological University, Xi'an, 710021, China
Guo-Sheng Qin, **Ke-Xuan Wang:** Shaanxi Applied Physics and Chemistry Research Institute, Science and Technology on Applied Physical Chemistry Laboratory, Xi'an, 710061, China

Keywords: photon Doppler signal, low signal-to-noise ratio, spectrum refinement and filter, weak beat frequency extraction

1 Introduction

Based on the optical Doppler effect, photon Doppler velocimetry (PDV) technology is the most widely used noncontact, ultra-high-speed micro-target velocity measurement technology suitable for transient, high-speed measurement scenarios such as blasting [1]. A fiber optic probe emits a reference light to a moving object, and the same probe receives the signal light reflected from the object. There is a certain beat frequency between the frequency of the light wave received by the probe and the frequency of the emitted light wave, and the size of the beat frequency is related to the target's speed in the direction of motion [2]. The amplitude of the photon Doppler signal changes periodically with time, and each period corresponds to a stripe. The frequency with the largest amplitude is the beat frequency, and the time interval corresponding to the maximum value of the stripe is the beat frequency period.

Extracting the beat frequency of the photon Doppler signal by short-term Fourier transform (STFT) is a common method. In the absence of high-frequency noise interference, the beat frequency is the only single peak spectrum in each window function spectrum [3]. The beat frequency curve of the Doppler signal is obtained by extracting each window spectrum's maximum amplitude spectrum frequency. However, when using PDV technology to measure tiny high-speed (V > 1,000 m/s) targets in engineering experiments, due to the influence of detection environment vibration, the acquired Doppler signal spectrum often contains a large amount of high-frequency noise, resulting in an extremely low signal-to-noise ratio (SNR < 0) [4]. The high-frequency noise and photon Doppler signal will be mixed acquisition, so it was not easy to filter out accurately. Assume that the beat frequency amplitude in the window spectrum is smaller than

the high-frequency noise amplitude. In that case, directly extracting the maximum spectral frequency will lead to serious errors since it is high-frequency noise and not beat frequency. Therefore, the reliability of the beat frequency depends on the accuracy of extracting the peak spectral position [5]. Extracting the weak beat frequency submerged by noise from the window spectrum is a technical difficulty and key [6].

The key to weak signal detection techniques is to eliminate interfering noise while protecting the target signal [7]. The most common method to extract weak signal features is to denoise the signal as much as possible [8]. Liu *et al.* [9] used an autocorrelation-based stacking method for denoising weak microseismic signals. However, this method made the signal amplitude attenuate seriously and difficult to recover. As the noise power increases, the autocorrelation of the target signal gradually decreases, so it is unsuitable for weak Doppler signals. Mengyao *et al.* [10] proposed to combine with sparsity adaptive compressive sensing and clustering algorithms to deal with the heterodyne signal of photon echo. However, the clustering algorithm is suitable for suppressing the Gaussian white noise of the signal. Guo *et al.* [11] removed noise using the wavelet threshold denoising algorithm, which is suitable for removing low-frequency noise with relatively uniform energy distribution in the frequency domain. Li *et al.* [12] used the power spectral subtraction algorithm to reduce signal noise, but this method is difficult to suppress the interference of nonstationary high-frequency noise.

To accurately extract the weak beat frequency of Doppler signals, it is necessary to ensure that the amplitude characteristics of Doppler signals are not affected during denoising [13]. However, the noise spectrum is disordered in the window function spectrum. The conventional denoising method cannot remove high-frequency noise interference while preserving the beat frequency characteristics. Therefore, this article fully considers the positioning and protection of the beat frequency characteristics without changing the spectrum amplitude. After data optimization, the target signal characteristics are more obvious in the refined narrowband spectrum after filtering out the interference spectrum band range, allowing the weak beat frequency to be accurately extracted.

2 Photon Doppler signal analysis and optimization method

2.1 Influence of high-frequency noise on Doppler signal

Figure 1 shows the system diagram of the PDV device. The laser is a 1,550 nm 5 kHz narrow linewidth laser with a maximum power of 1 W. The reference and signal light form a Doppler frequency-shifted interference signal at the 1 × 2 coupler and are acquired by the oscillograph.

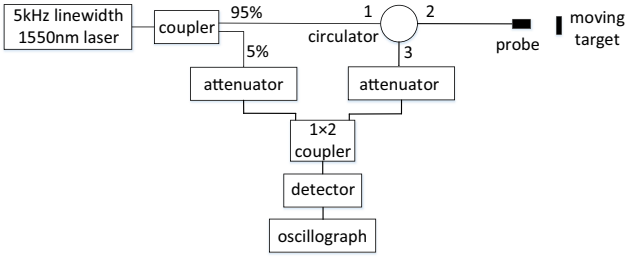

Figure 1: System diagram of PDV device.

When processing the signal by STFT, the STFT converts signals within the length of the window into the frequency domain by selecting a time-to-frequency conversion window function and moving the window function over the signal. To reduce the fence effect of the discrete spectrum, one can either directly select a window function with a large attenuation of the first side lobe or suppress the side lobe by self-convolution of the window function [14]. The time and frequency resolution of the STFT depends on the size of the window length. The longer the window, the longer the intercepted signal, the lower the time resolution, and the higher the frequency resolution, which are inversely related. Therefore, the appropriate window length is selected according to the sampling frequency, and the window length is normalized. To comply with the Nyquist sampling theorem, the sampling frequency can be usually set to the same value as the signal acquisition frequency.

The PDV device measures the velocity of tiny flying fragments after an explosion. Figure 2 shows two sets of

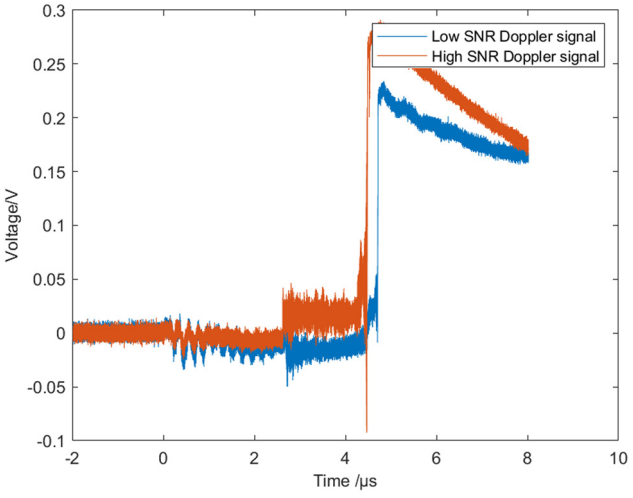

Figure 2: Two sets of photon Doppler shifted voltage signals.

photon Doppler-shifted voltage signals from the explosion experiment. The sampling frequency is 2×10^{10} Hz, and the acquisition card can collect 20,000 data points in 10 μs. Figure 3 shows the beat frequency curve of the low SNR Doppler signal shown in Figure 2, and there are obvious outliers in the curve affected by high-frequency noise. The method [15] of correcting the different regions' frequency spectrums according to the noise interference intensity can only provide an estimated value of weak beat frequency completely submerged in high-frequency noise. Therefore, further window spectrum analysis is required to obtain accurate beat frequency values.

Figures 4 and 5 show the window function spectrum for the 8th and 10th outlier beat frequencies shown in Figure 3, respectively. It can be seen that the spectrum is heavily disturbed by noise, and the noise spectrum is disordered. When the amplitude of the noise spectrum is much larger than the beat frequency, directly extracting the maximum amplitude spectrum frequency will lead to serious errors. Therefore, after STFT processing, it is difficult to extract the weak beat frequency directly, which is completely overwhelmed by high-frequency noise.

2.2 Weak beat frequency extraction method

To accurately extract the weak beat frequency from the noise spectrum, the amplitude characteristics of the Doppler signal need to be unaffected in the denoising process. This article first uses the Kalman filter to obtain the optimal estimate between the initial and predicted values of the beat frequency. The estimated beat frequency obtained approximates the exact beat frequency, which provides a suitable passband center frequency f_e for multiple analytical bandpass filters. The multiple analytical bandpass filter uses f_e as the passband's center and refines the spectrum of the Doppler signal in the narrow band range ($f_1 \sim f_2$). This method can directly filter out other interference bands, refine the spectrum near the beat frequency, and make the amplitude characteristics of the weak beat frequency more obvious in the narrow band range.

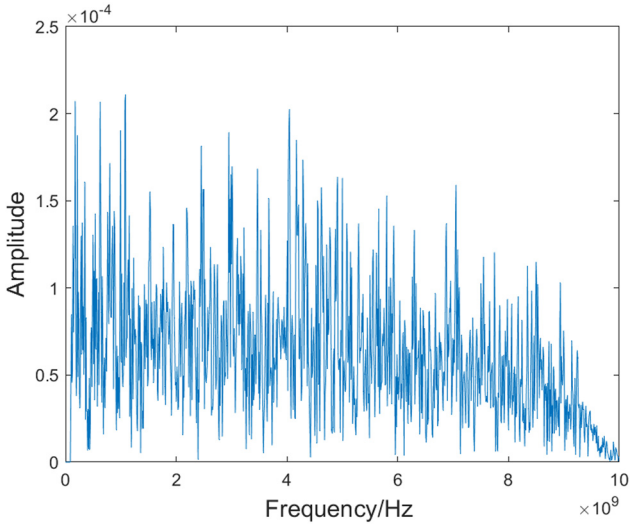

Figure 4: Spectrum diagram of the 8th window function.

2.2.1 Design of multiple analytical bandpass filter

The design method of multiple analytical bandpass filters is to perform complex frequency shifts on the real low-pass

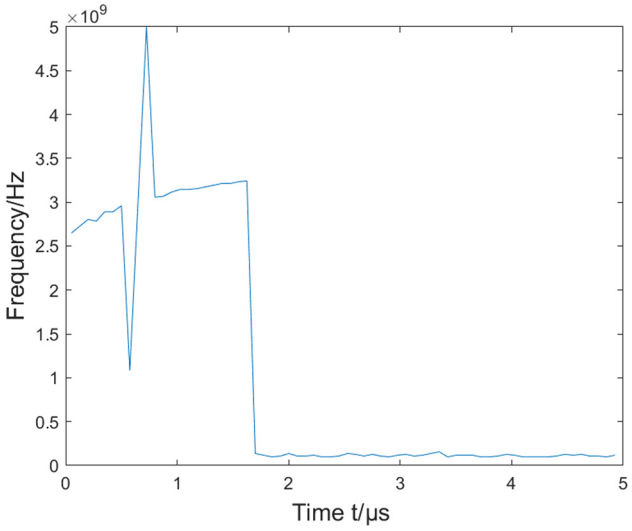

Figure 3: Beat frequency curve of low SNR Doppler signal.

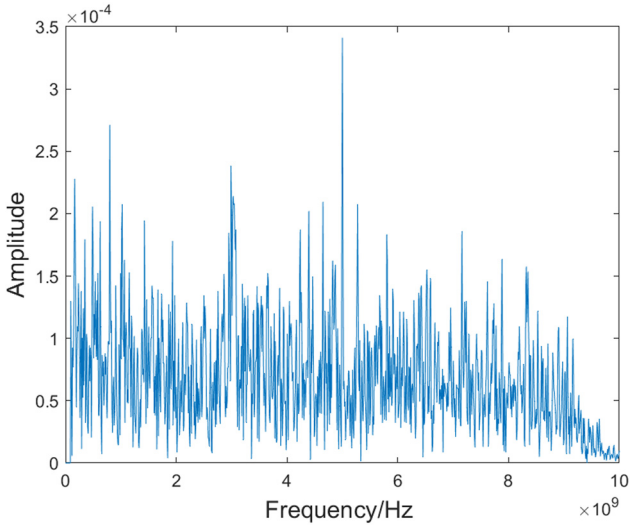

Figure 5: Spectrum diagram of the 10th window function.

filter and move the passband center from 0 to ω_e^1, and the passband width of the low-pass filter is $\omega_2^1 - \omega_1^1$ [16]. The shock response function $h^0(k)$ of the multiple analytical bandpass filter is a complex number with a real part h_R^0 and an imaginary part h_I^0, as shown in Eqs. (1) and (2). The real part is even symmetric, and the imaginary part is odd symmetric, so only half of the sequence needs to be computed, where the amplitude of the bandpass part is two and M is the half order of the filter.

$$h_R^0(k) = \frac{1}{\pi k}[\sin(k\omega_2^1) - \sin(k\omega_1^1)]; \quad k = -M, -M + 1, \ldots, -1, 0, 1, \ldots, M, \tag{1}$$

$$h_I^0(k) = \frac{1}{\pi k}[\cos(k\omega_1^1) - \cos(k\omega_2^1)]; \quad k = -M, -M + 1, \ldots, -1, 0, 1, \ldots, M. \tag{2}$$

Multiple analytical bandpass filter usually requires adding half of the window function to improve the passband's flatness and the stopband's ripple effect. Commonly used window functions are rectangular window, Hanning window, and Hamming window. To reduce the fence effect of the discrete spectrum, the first side lobe attenuation degree and the descent rate of the side lobe are considered when choosing the window function. The Hanning window has a first side lobe attenuation of up to 31 dB and a side lobe descent rate of 18 dB/octave.

After adding the Hanning window to the low-pass filter corresponding to the multiple analytical bandpass filter generated by Eqs. (1) and (2), the spectrum of its half-passband interval $(0, \omega_c)$ is shown in Figure 6 [17]. Point C is the ideal bandpass boundary with an amplitude of 0.5. Section AB is the transition zone with a width of ω_p, AC is the inner transition zone, and CB is the outer transition zone. a_1,a_2, and a_3 represent the peaks of side lobes. Stopband filtering starts at point B, and point E's right side completely stops filtering. A good band-stopping effect can be obtained from C to B and then double the extension of the outer transition zone to point E.

Figure 7 shows the design diagram of the transition zone after D down-sampling. D is the refinement factor. Draw the transition zone AB as a straight line, where $B'B$ is the frequency mixing zone. The transition band midpoint C is the filter design boundary, so the passband boundary needs to be extended from A to point D. Making the refined band interval $(0, \pi)$ represented by the shaded region all within the straight line segment of the passband is called the extension of the passband design boundary.

The filter length (order) as well as the window function's length is $2M + 1$. The window function length is inversely proportional to the main lobe width of the window spectrum. The total transition bandwidth ω_p equals the window spectrum's main lobe width. So, the relationship between the half-order M of the filter and the transition bandwidth ω_p^1 is also inversely proportional, as shown in Eq. (3).

$$\omega_p^1 = 4\pi/M. \tag{3}$$

The horizontal coordinate ω^1 before D down-sampling expands D times compared to the horizontal coordinate $\overline{\omega}^1$ after down-sampling. Set the width of the transition zone before D down-sampling as $\overline{\omega}_p^1$, and after down-sampling, the transition zone ω_p^1 will be compressed by D times. ω_p^1 is shown in Eq. (4).

$$\omega_p^1 = \overline{\omega}_p^1/D = a\pi/D, \ a > 0. \tag{4}$$

According to Eqs. (3) and (4), when determining the external spreading coefficient a, the relationship between the half-order M and the refinement factor D can be obtained, as shown in Eq. (5).

$$M = 4D/a. \tag{5}$$

As long as point A in Figure 7 is within the range $[\pi, 1.5\pi]$, the refined band interval $(0, \pi)$ can all be within the straight line segment of the passband. When $a \in [2/3, 1.2]$, this requirement is usually met and no amplitude corrections are needed at both ends of the refined band spectrum. Therefore, in the case of determining the external spreading coefficient a, the

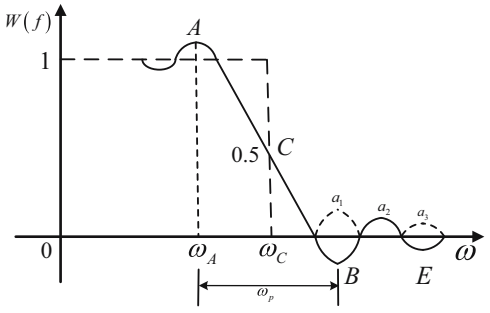

Figure 6: Transition band design of the low-pass filter.

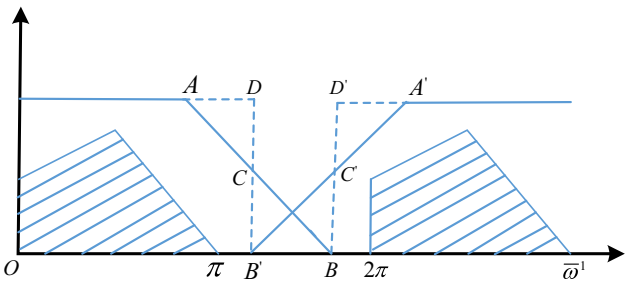

Figure 7: Design diagram of D down-sampling transition zone.

refinement factor D, the multiple analytical bandpass filter can be generated according to Eqs. (1) and (2).

2.2.2 Multiple modulation zoom spectrum

The signal $x(n)(n = 0, 1, 2,\ldots,DN + 2M)$ is down-sampled by constructing a multiple analytical bandpass filter $h^0(n)$ with an ideal passband width $f_s/(2D)$. Select a sampling point at intervals of $2D$ points, the number of sampling points is N, and the sampling frequency is $f_s/(2D)$. After determining the center frequency f_e, the passband width $[-f_s/(4D), f_s/(4D)]$ corresponds to the refined analysis interval $[f_1, f_2]$ [18,19]. Therefore, Eq. (6) shows the relationship between the analysis interval $[f_1, f_2]$ and the refinement factor D.

$$D = f_s/(f_2 - f_1). \tag{6}$$

After the real signal passes through multiple analytical bandpass filters, it becomes a complex analytical signal $\overline{x}(n)$ with a frequency in the range of $(f_1 \sim f_2)$. Through the complex carrier signal $s(n)$, the starting frequency of the refined complex signal $\overline{x}(n)$ is moved to the zero frequency point to obtain the complex modulation signal $\overline{y}(n)$, and the frequency shift $\overline{\omega}_1^1$ is expressed as follows:

$$\overline{\omega}_1^1 = 2\pi D f_1/f_s. \tag{7}$$

The complex modulation signal $\overline{y}(n)$ is expressed as follows:

$$\overline{y}(n) = \overline{x}(n)s(n) = \overline{x}(n)e^{-j\overline{\omega}_1^1 n}, \quad n = 0,\ldots,N-1. \tag{8}$$

Then $N/2$ points FFT spectrum analysis on $\overline{y}(n)$ and takes the positive frequency part. Without frequency adjustment, the spectrum of the refined frequency band $(f_1 \sim f_2)$ can be represented by $N/2$ independent spectral lines.

2.2.3 Provide passband center frequency based on Kalman filter

The high-speed photon Doppler beat frequency curve is a one-dimensional variable. Because the time unit is on the order of microseconds, the beat frequency values at adjacent moments are close in the case of high-frequency resolution. Therefore, the beat frequency value at the k moment can be estimated using the beat frequency value at the $k-1$ moment. The state equation is shown in Eq. (9), and the observation equation is shown in Eq. (10). The initial beat frequency $F_{\text{beat}}(k)$ is extracted by STFT, the system models A and H are set to 1, and the measurement noise $V(k)$ is greater than the process noise $W(k)$.

$$X(k) = A \cdot F_{\text{beat}}(k-1) + W(k-1), \tag{9}$$

$$Z(k) = H \cdot X(k) + V(k). \tag{10}$$

The weak beat frequency extraction method is as follows:

1) The photon Doppler signal is processed by STFT, the window length is normalized, and then each window spectrum's maximum amplitude spectrum frequency is extracted to obtain the initial beat frequency value.
2) The Kalman filter is used to optimally estimate the initial beat frequency value so that the estimated value is close to the actual beat frequency, which provides a suitable passband center frequency f_e for multiple analytical bandpass filters.
3) Construct a multiple analytical bandpass filter and determine parameters such as refinement factor D, external spreading coefficient a, number of sampling points N, and down-sampling frequency f_s.
4) After multiple analytical bandpass filters process the weak signal, each refined narrow band's maximum amplitude spectrum frequency is extracted to obtain the beat frequency value after data optimization.

3 Experimental signal data processing

3.1 Low SNR signal data processing

How the algorithm is used will be illustrated in detail using the low SNR Doppler shifted voltage signal in Figure 2. A multiple analytical bandpass filter of width $f_s/(2D)$ is first constructed, and a sampling point is selected at intervals of $2D$ points. The number of sampling points is $N/2$, let N be 512, and the down-sampling frequency $f_s/(2D)$ must conform to the Nyquist sampling theorem. The value of the sampling frequency f_s is set to 2×10^{10} Hz, the same as the acquisition frequency of the photon Doppler signal. Refinement factor D is set to 3. The external spreading coefficient a is 1.2. The filter half-order M can be calculated by Eq. (5). The upper and lower bounds of the extended bandpass filter are computed using the estimated beat frequency value of the Kalman filter as the passband center. Then, the multiple analytical bandpass filter is generated by Eqs. (1) and (2), and finally, half of the Hanning window is added to form the transition band.

Weak signals are selectively sampled and filtered by the multiple analytical bandpass filter, and the signal length must be greater than or equal to $N \cdot D + 2M$. Through data processing, the spectrum of each window takes the optimal estimated beat frequency value of the Kalman

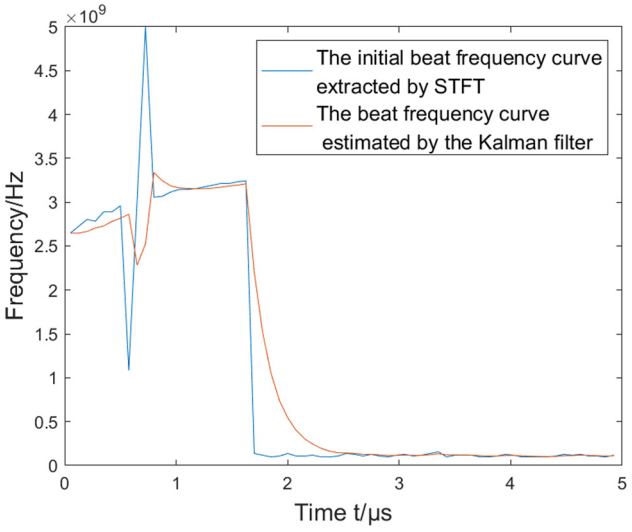

Figure 8: The beat frequency curve estimated by the Kalman filter based on the initial beat frequency curve.

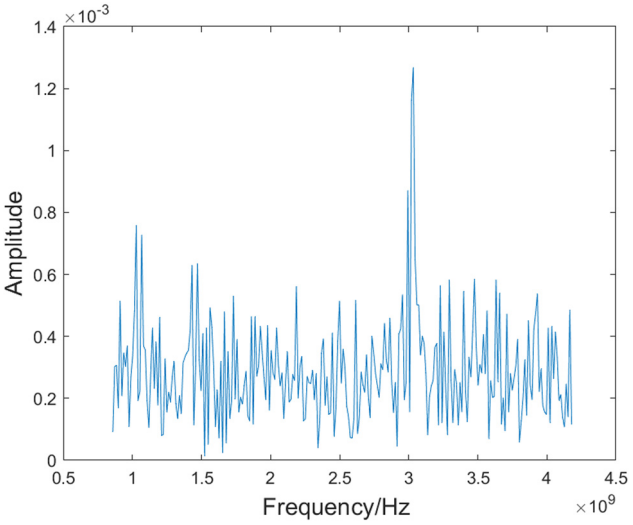

Figure 10: Filtering and refinement spectrum of the 10th window function.

filter as the passband center with 256 spectral lines, reflecting a refined bandwidth of 3.3×10^9 Hz. Beat frequency values are obtained by extracting the maximum amplitude spectrum frequency of each refined and filtered windowed spectrum.

Figure 8 shows the initial high-noise Doppler beat frequency curve extracted by STFT and the beat frequency curve estimated by the Kalman filter based on the initial beat frequency curve. It can be seen that the beat frequency curve estimated by Kalman filtering is relatively smooth and conforms to the growing trend of the initial beat frequency curve but greatly reduces the error of the abnormal beat frequency values, which can be regarded as a filtering process, such as the beat frequency estimated in the 8th and 10th window functions spectrum. Therefore, the passband center frequency can be provided for the multiple analytical passband filter.

The filtering and refinement spectrum of the 8th and 10th window functions are shown in Figures 9 and 10, respectively. The filtering and refinement spectrum bandwidth is all 3.3×10^9 Hz, but the spectrum band's center frequency changes with the Kalman filter's estimated beat frequency value.

As shown in Figure 11, by comparing the 10th window function spectrum before and after data optimization, this

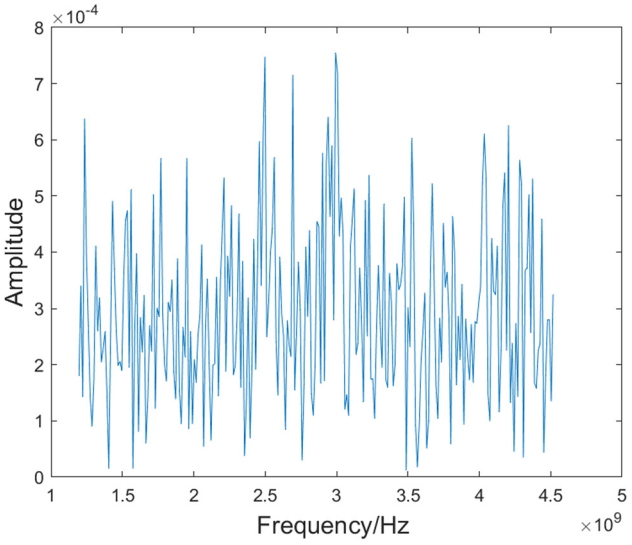

Figure 9: Filtering and refinement spectrum of the 8th window function.

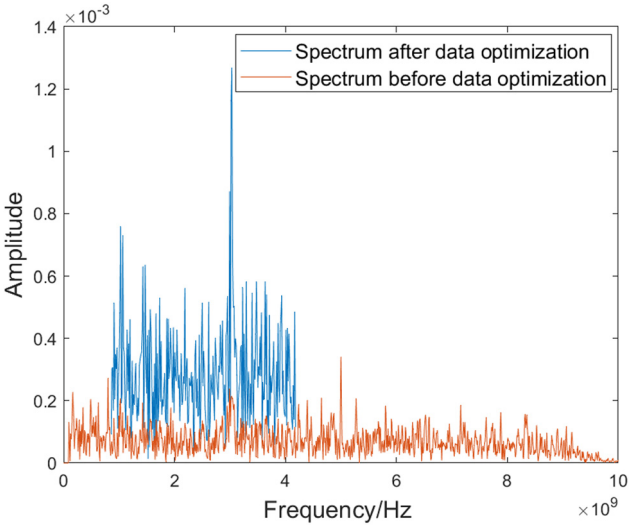

Figure 11: The 10th window function spectrum of before and after data optimization.

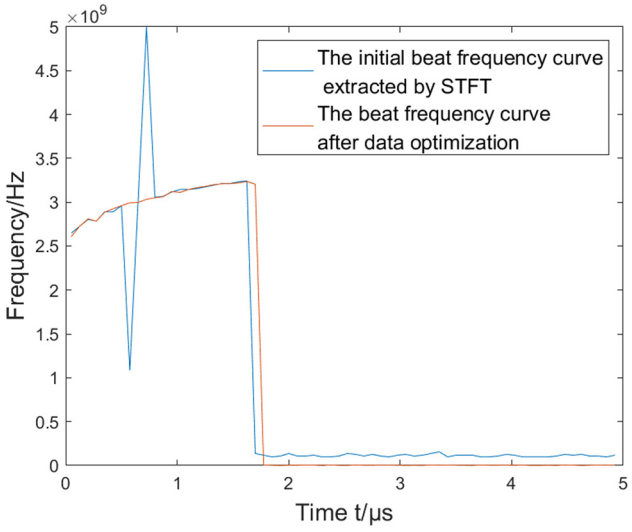

Figure 12: The comparison of low SNR Doppler beat frequency curve before and after data optimization.

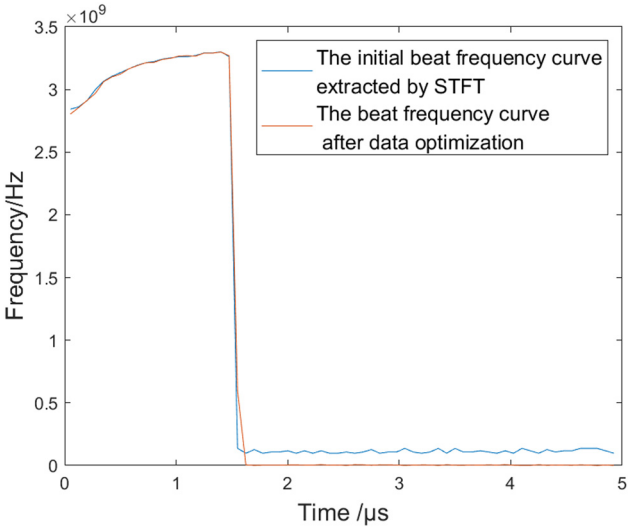

Figure 14: The comparison of high SNR Doppler beat frequency curve before and after data optimization.

data optimization method can directly filter out the interference of unrelated spectrum bands and accurately refine the spectrum near the beat frequency signal. In the narrow band range, the amplitude characteristics of the Doppler signal are more evident.

As shown in Figure 12, the beat frequency curve is stable and smooth after data optimization. The beat frequencies of the 8th and 10th window function spectrum, completely drowned by noise in the initial beat frequency curve, can also be extracted accurately.

3.2 High SNR signal data processing

The algorithm's reliability is verified by the high SNR Doppler signal in Figure 2. As shown in Figure 13, the initial beat frequency curve has been relatively smooth by STFT, and the Kalman filter estimated beat frequency curve is close to the initial beat frequency curve. The signal is refined and filtered by constructing multiple analytical bandpass filters with the beat frequency value estimated by the Kalman filter as the passband center. Then, the maximum amplitude frequency of each narrowband window spectrum is extracted.

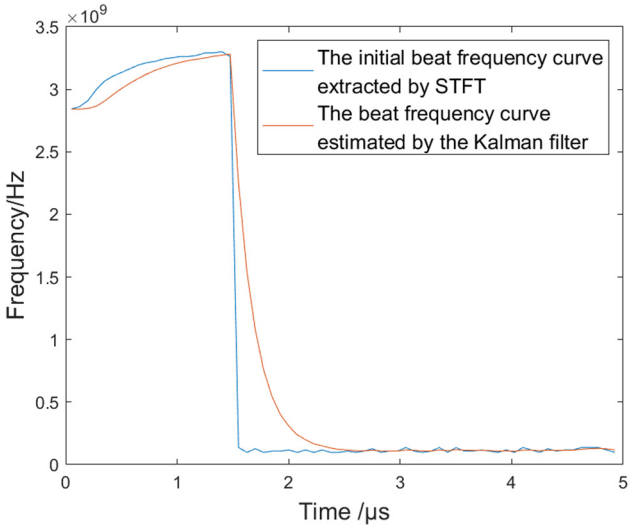

Figure 13: The beat frequency curve estimated by the Kalman filter based on the initial beat frequency curve.

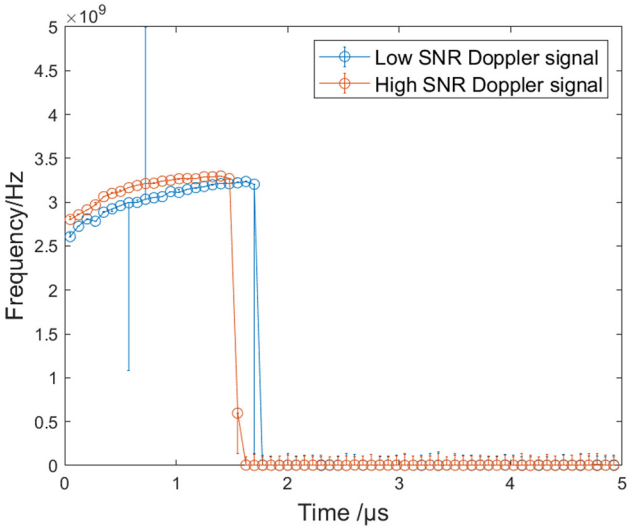

Figure 15: Error bar chart of two sets of photon Doppler signals.

Table 1: Eight sample points before and after data optimization starting from 0.5 μs in Figure 14

Sample point	1	2	3	4	5	6	7	8
Low SNR signal initial beat frequency/GHz	2.959	1.084	3.027	5.000	3.057	3.066	3.115	3.145
Beat frequency after data optimization/GHz	2.960	2.993	2.997	3.033	3.050	3.063	3.121	3.111
High SNR signal initial beat frequency/GHz	3.135	3.164	3.193	3.213	3.223	3.242	3.252	3.262
Beat frequency after data optimization/GHz	3.123	3.165	3.190	3.212	3.216	3.240	3.249	3.267

As shown in Figure 14, the beat frequency curve after data optimization almost coincides with the initial beat frequency curve, but the beat frequency value after data optimization is more accurate.

3.3 Comparison of errors before and after data optimization

Figure 15 shows the error bars of two sets of photon Doppler signals. Among them, the low SNR Doppler signal shows that the error is significantly reduced after data optimization for the beat frequency signal completely submerged by high-frequency noise. In addition, the high SNR Doppler signal verifies the algorithm's reliability.

Table 1 shows eight sample points of beat frequency values before and after data optimization of the low and high SNR Doppler signal starting from 0.5 μs in Figure 15. The relative error ε is calculated as shown in Eq. (11). Divide the absolute value of the difference between the pre-optimization value X_b minus the postoptimization value X_a by the postoptimization value.

$$\varepsilon = \frac{|X_b - X_a|}{X_a}. \tag{11}$$

Observing the beat frequency values in the second and fourth groups of low SNR signal showed that the beat frequency values with the most serious errors were reduced by 63.8 and 64.9%, respectively, after data optimization. According to the classical velocity demodulation equation [20], the wavelength is 1,550 nm, and this algorithm maximum can reduce the instantaneous error of 1,524 m/s. By observing the high SNR signal, the data-optimized beat frequency can be accurate to 10^6Hz, equivalent to 0.775 m/s after speed demodulation.

4 Conclusions

When the photon Doppler signal is interfered with by high-frequency noise, it is difficult to extract the weak beat frequency completely submerged in the noise by conventional denoising methods. Therefore, this article first estimates the value of the beat frequency by the Kalman filter and then builds a multiple analytical bandpass filter to refine the spectrum of the high noise signal with the value of the beat frequency estimate as the spectrum band center. This technique only extracts the beat frequency from the narrowband refinement spectrum by removing the interference spectrum band range. Therefore, it is possible to accurately extract weak beat frequency completely submerged in noise while preserving the amplitude characteristics of the Doppler signal. We introduce the use method of this algorithm through low SNR photon Doppler signals, with a maximum beat frequency error reduction of 64.9%. The high SNR photon Doppler signal verifies the algorithm's reliability, and the beat frequency accuracy can reach 10^6 Hz after data optimization. The advantage of this algorithm is that it is repeatable and makes the characteristics of weak beat frequency more prominent by removing the interference spectrum band range without changing the amplitude characteristics of the Doppler signal, thus avoiding the errors caused by affecting the spectrum amplitude in conventional denoising methods.

Funding information: This work was supported by Science and Technology on Applied Physical Chemistry Laboratory, China (Grant No. WDYX21614260202).

Author contributions: All authors have accepted responsibility for the entire content of this manuscript and approved its submission.

Conflict of interest: The authors state no conflict of interest.

Data availability statement: The data that support the findings of this study are available from the corresponding author upon reasonable request.

References

[1] Jensen BJ, Holtkamp DB, Rigg PA, Dolan DH. Accuracy limits and window corrections for photon Doppler velocimetry. J Appl Phys. 2007;101(1):3523.

[2] Son J-T, Lee S-H, Park K-H. Instantaneous frequency estimation of doppler signal using wavelet transform. J Inst Electron Eng Korea SP Signal Process. 2005;42(3):99.
[3] Chen Z, Rettinger R, Hefferman G. Microwave-modulated photon doppler velocimetry. IEEE PTL. 2016;28(3):327–30.
[4] Jianhong Z, Jinhui W, Gao W, Ji L, Ninggang S, Yuan J. Method for velocity reconstruction of Doppler radar projectile velocity signal. China Meas Test. 2020;46(4):31–5.
[5] Wei-Lung M, An-Bang C. New code delay compensation algorithm for weak GPS signal acquisition. AEU-Int J Electron C. 2009;63(8):665–7.
[6] Kang C, Chenghao J, Jingguo Z, Juan D, Zhi Q, Zhengyu Y. Frequency shift characteristics of laser Doppler effect. Infrared Laser Eng. 2021;50(11):150–7.
[7] Chao W, Erxiao L, Zhihua J. Two-step compressed acquisition method for Doppler frequency and Doppler rate estimation in high-dynamic and weak signal environments. J Syst Eng Electron. 2021;32(4):831–40.
[8] Deng T, Ma M, Liu Q, Wu Y. High-precision carrier tracking algorithm for extremely weak and high-dynamic signals. Radio Sci. 2021;56(5):e2021RS007277.
[9] Liu E, Zhu L, Govinda Raj A, McClellan JH, Al-Shuhail A, Kaka SI, et al. Microseismic events enhancement and detection in sensor arrays using autocorrelation-based filtering. Geophys Prospect. 2017;65(6):1496–509.
[10] Mengyao P, Yihua H, Fanghui Q, Xinyuan Z, Xiao D. Signal processing method of photon echoes heterodyne for variable-speed target. Chin J Lasers. 2023;50(10):230–40.
[11] Guo H, Yue L, Song P, Tan Y, Zhang L. Denoising of an ultraviolet light received signal based on improved wavelet transform threshold and threshold function. Appl Opt. 2021;60(28):8983–90.
[12] Li Y, Zhao X, Wang J, Xi X, Li D. Long-distance laser Doppler water flow velocimetry method based on adaptive Gaussian weighted integration. Appl Opt. 2023;62(6):A1–11.
[13] Nezhadshahbodaghi M, Mosavi MR, Rahemi N. Improved semi-bit differential acquisition method for navigation bit sign transition and code doppler compensation in weak signal environment. J Navig. 2020;73(4):892–911.
[14] Yanlin W, Yunbo S, Qiang K, Zhenguo M, Jie Z, Huiliang C. Frequency extraction and correction based on double window all phase FFT of laser Doppler. Laser Infrared. 2019;49(12):1395–401.
[15] Sun YN, Wu SJ, Wang J, Li DJ, Du YQ, Mei D. Beat frequency extraction method of high speed and high noise Doppler signal based on double correction. Opt Eng. 2023;62(2):028102.
[16] Shuohan MA, Qishuang MA, Xinbo L. Applications of chirp z transform and multiple modulation zoom spectrum to pulse phase thermography inspection. NDT E Int. 2013;54(000):1–8.
[17] Kang D, Ming X, Bide Z, Ling Z, Xiaofei Z. Algorithm of multiple modulation zoom spectrum analysis based on complex analytic bandpass filter. J Vib Eng. 2001;14(01):33–9.
[18] Ming X, Kang D. Principle and method of multiple modulation zoom spectrum analysis based on multiple analytical bandpass filter. J Vib Eng. 2002;15(04):111–5.
[19] Zhang Q, Cai X, Li W, Liu Z, Meng X. A detection method of dense harmonics/inter-harmonics based on improved all-phase time-shifting method and zoomFFT. J Phys Conf Ser. 2021;1750(1):012013 (7pp).
[20] Mallick DD, Zhao M, Bosworth BT, Schuster BE, Foster MA, Ramesh KT. A simple dual-beam time-multiplexed photon doppler velocimeter for pressure-shear plate impact experiments. Exp Mech. 2019;59(1):41–9.